

COMPOSITE MATERIALS FOR INNOVATIVE WIND TURBINE BLADES*

Thomas D. Ashwill and Joshua A. Paquette
Wind Energy Technology Department
Sandia National Laboratories†
Albuquerque, NM 87185

ABSTRACT

The Wind Energy Technology Department at Sandia National Laboratories (SNL) focuses on producing innovations in wind turbine blade technology to enable the development of longer blades that are lighter, more structurally and aerodynamically efficient, and impart reduced loads to the system. A large part of the effort is to characterize the properties of relevant composite materials built with typical manufacturing processes. This paper provides an overview of recent studies of composite laminates for wind turbine blade construction and summarizes test results for three prototype blades that incorporate a variety of material-related innovations.

KEY WORDS: Carbon Fiber Composites, Failure Criteria/Failure Mechanisms, Fatigue/Fatigue Resistance, Glass Fiber Composites, Prepreg Materials/Prepreg Properties, Resins/Materials–Epoxy, Resins/Materials–Polyester/Vinyl Ester, Testing/Evaluation, Wind Turbine Blade Technology

1. INTRODUCTION

Installed wind energy capacity both worldwide and in the U.S. has grown exponentially over the past few years. Figure 1 (1) shows the yearly and cumulative installed capacity in the United States from 1995 to 2006, with 2007's entry as an estimate. The 2007 number actually came in at 5.2 GW, as reported by AWEA (www.awea.org), well ahead of the estimated 3.4 GW.

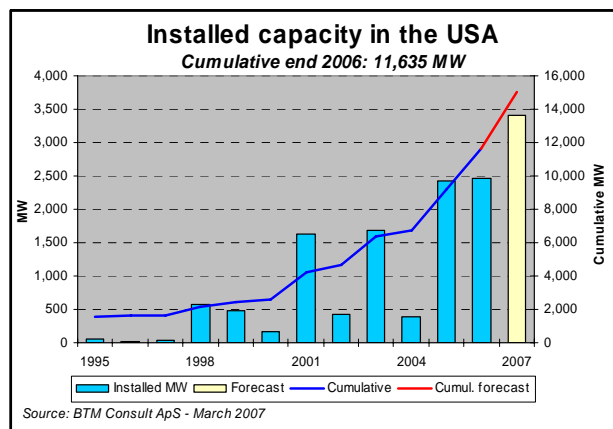


Figure 1: U.S. Installed, Utility-Grade Wind Energy Capacity

* This paper is a work of the U.S. Government and is not subject to copyright protection in the United States.

† Sandia is a multiprogram laboratory operated by Sandia Corporation, a Lockheed Martin company, for the U.S. Department of Energy under contract DE-AC04-94AL85000

The U.S. demand for new turbines is up dramatically, especially in the last three years in large part due to the continued activation of the Production Tax Credit (PTC). The inflation-adjusted COE for wind power has fallen dramatically as well (at least up until the last two years when turbine demand and extra-high commodity price rises took effect). A large part of this drop has to do with the inherent efficiencies associated with larger turbines. The physical size has grown from an average of 100 kW in 1985 to over 1.5 MW today (2008).

1.1 Innovation Development SNL is developing concepts that will enable the utilization of longer blades that weigh less, are more structurally and aerodynamically efficient, and impart reduced loads to the system (2).

One of the primary goals for blade research is to keep blade weight growth under control. For cantilevered beams, which turbine blades can be approximated as, root loads caused by gravity approximately scale as the cube of the blade length. As turbines continue to grow, these gravity loads become more of a constraining design factor. That is, unless the increase in blade weights can be contained by more efficient design methodology. Figure 2 shows blade weight growth trends as a function of rotor radius from commercial data and WindPACT preliminary designs (3). Here we can observe trend lines of older commercial designs, newer commercial designs, and designs that have come out of the DOE-sponsored WindPACT studies (4) that incorporate new concepts. The figure shows that it is possible to lower the growth rate from an exponent of 3.0 to as low as about 2.5.

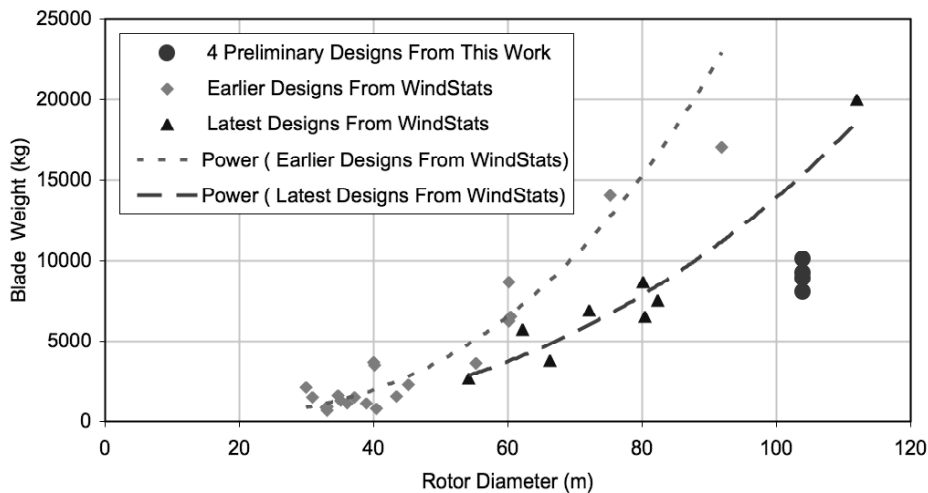


Figure 2: Blade Weight vs. Rotor Diameter

1.2 Specific Concepts Examples of the concepts that SNL is developing include:

1. More efficient blade structures (thick airfoils, designs that fully integrate structure and aerodynamics, and slenderized blade geometries)
2. Adaptive structures (passive bend-twist coupling and active devices)
3. Materials, fatigue and manufacturing
 - a. New materials for wind turbine blades such as carbon, carbon-hybrid, S-glass and new material forms
 - b. Design details to minimize stress concentrations in ply drop regions
 - c. Less expensive, embedded blade attachment devices

For this paper we will concentrate on discussing recent results in the areas of composite material research and the testing of three subscale prototype blades that employ material and structural innovations. Section 2 summarizes recent SNL-sponsored material fatigue testing performed at Montana State University (7,8). Section 3 provides highlights of the SNL/GEC Blade System Design Study-Phase II research contract that tested a variety of carbon and carbon-hybrid materials (9). Section 4 provides an overview of ongoing testing activities in the SNL 9-m prototype research program (35,36).

2. MSU COMPOSITE COUPON TESTING, CIRCA 2007-08

For many years, SNL has had an ongoing effort to characterize composite materials for wind turbine use. Much of the related fatigue testing of composite materials has been and continues to be performed by Montana State University (MSU), which first published the DOE/MSU Composite Material Fatigue database in 1997 (5,6). This document, which is updated yearly, contains the results of static and fatigue coupon testing of commercially-available composite materials.

2.1 Recent Selected Fatigue Results

2.1.1 Effects of Fiber Type The effects of fiber type on tension and compression fatigue resistance are shown in Figure 3, where the stress and strain based fatigue resistance in tension ($R = 0.1$) and compression ($R = 10$) are compared (7,8).

The four laminates, representing three main fiber types all with epoxy resins, are

- E-glass (or Advantex™), QQ1
- E-LT- 5500-EP
- WindStrand™, WS1
- Carbon hybrid (Grafil 34-600, 48k tow), P2B

(See Appendix A for more details on these material specifications). The laminates have differing contents of 0° plies relative to $\pm 45^\circ$ plies, slightly different fiber contents, and different processing. Notable differences in fatigue performance are that the carbon hybrid is superior in terms of stress, and shows a much higher fatigue exponent as compared to the glass fiber materials tested at $R = 0.1$ (tension-tension fatigue). The same can be said of the performance of carbon at $R = 10$ (compression-compression fatigue). Of the glass laminates, QQ1 is notably less fatigue resistant than E-LT-5500-EP in tension while the converse is true in compression. WindStrand™ is generally similar to the best of the E-glass laminates in each case, but slightly stronger in terms of stress, in tension. The aligned strand structure of the WindStrand™ WS1 laminates may be advantageous as compared with the stitched fabrics used for QQ1 and E-LT-5500 (9).

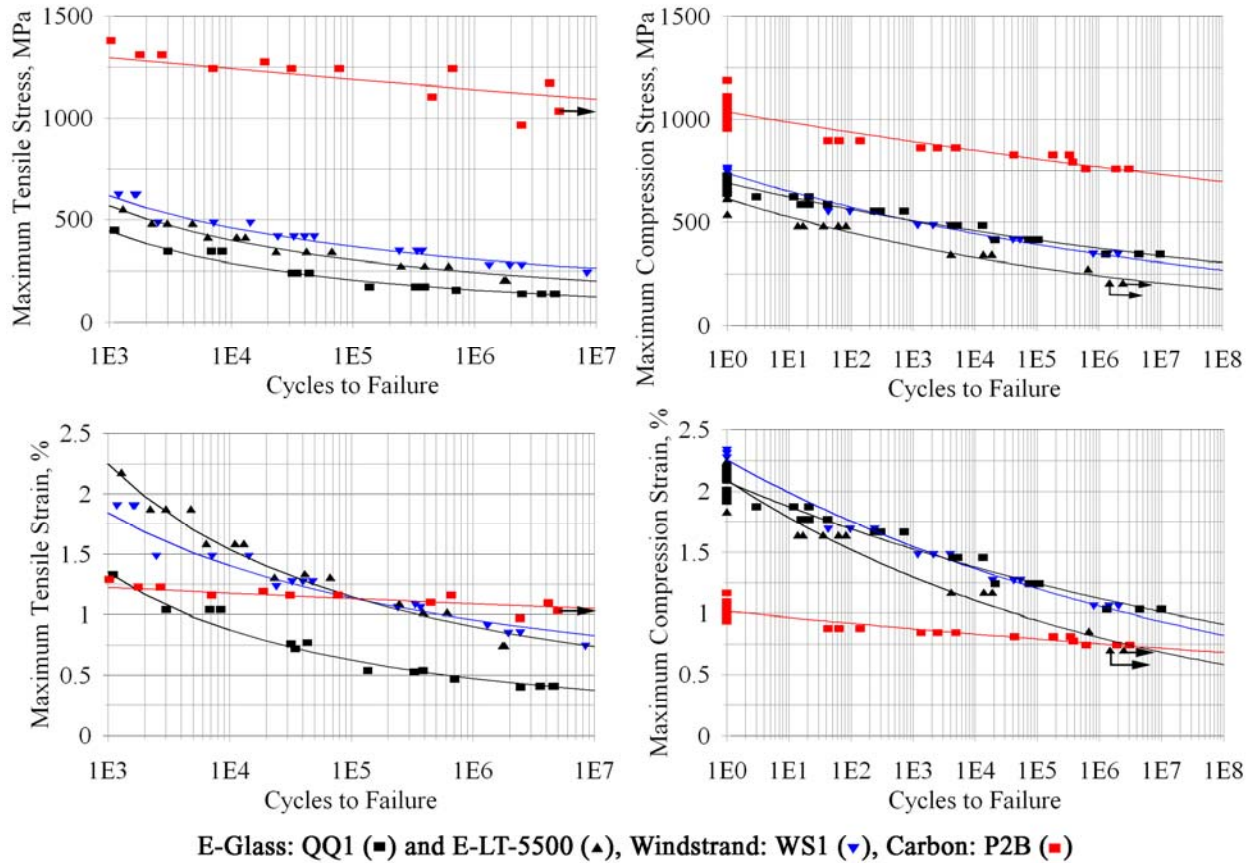


Figure 3: Fatigue comparison of multidirectional laminates based on E-glass (QQ1 and E-LT-5500), WindStrand™ (WS1) and carbon (P2B) fibers at similar fiber contents, in terms of stress (top) and strain (bottom), epoxy resins, $R = 0.1$ (left side) and $R = 10$ (right side).

2.1.2 Carbon Reinforcement Carbon hybrid laminates are compared in Figure 4. Carbon fiber reinforced laminates for wind blades are most limited by compressive strength and ultimate strain (10, 11). Additionally, the presence of even minor amounts of fiber misalignment has been shown to reduce static and fatigue properties significantly (12). Maximum compressive properties are obtained with laminates which have the straightest fiber alignment, generally unidirectional prepreg 0° plies; poorest properties have been found with woven fabrics, particularly with large tows. Figure 4 compares the compressive static and fatigue properties for three carbon fiber materials: P2B, relatively thick (0.3 mm) prepreg with unidirectional carbon fiber 0° plies; MMWK C/G-EP, infused triaxial fabric with $+45^\circ$ and -45° E-glass plies sandwiching 0° carbon strands; and CGD4, VARTM processed 0° stitched carbon fabric with E-glass $\pm 45^\circ$ plies. The P2B laminate gives properties typical of other large tow prepreps (9,10). The CGD4 laminate is among the best stitched or bonded carbon fabrics tested (10), but not as good as the prepreg, apparently due to slight misalignment in the fabric strands. The MMWK-C/G-EP laminate properties were at least equivalent to various prepreps tested in this program, with very straight strands held in place by the glass 45° 's. This fabric contains about 25% off-axis material by volume which reduces the strength and modulus values relative to 100% unidirectional carbon laminates (9).

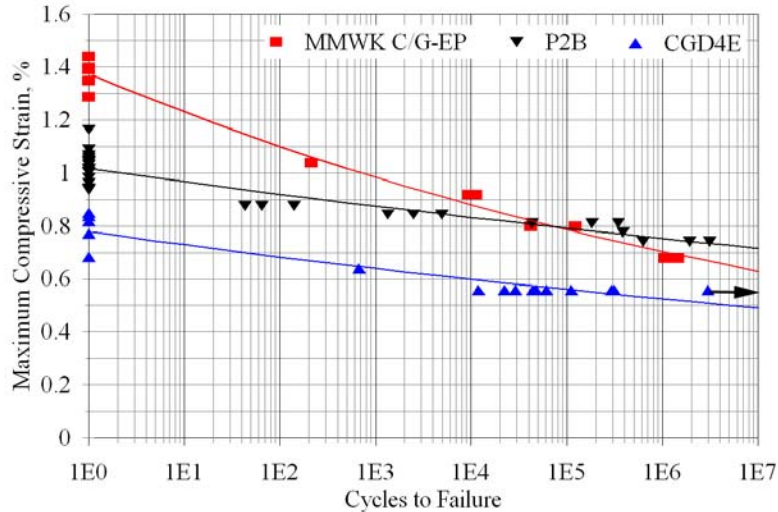


Figure 4: Comparison of compressive fatigue resistance of hybrid laminates with carbon 0° plies and E-glass $\pm 45^\circ$ plies: materials P2B (prepreg); MMWK C/G-EP (infused stitched hybrid triaxial fabric); and CGD4E (VARTM stitched fabrics) at $R = 10$.

2.2 Summary of Issues and Conclusions Major issues have been identified which can produce severe fatigue damage or failure in good quality coupons at maximum absolute strains in the range of 0.2 to 0.4%:

1. Glass fiber laminates with less fatigue resistant fabric architectures at higher fiber contents, loaded in tensile fatigue with R-values in the -0.5 to 0.1 range.
2. Delamination at ply drops and ply joints, for plies greater than 1.0 mm thickness for glass fibers, or 0.6 mm for carbon fibers (most R-values).
3. Matrix cracking in off-axis plies, for R-values with a significant tensile component (glass and carbon fiber laminates, various resins).
4. Carbon fiber laminate compressive strength and its sensitivity to fabric or other fiber waviness.
5. Delamination and adhesive failure in complex details under both static and fatigue loading.
6. Hot/wet conditions can exacerbate these issues (with the exception of the first).

Major conclusions are (see Refs. 8,9,13,14 for more detail):

1. The relatively new WindStrand™ based laminates, in addition to moderately higher modulus, show very good fatigue resistance under both tension and compression loading, compared to E-glass.
2. Carbon, either prepreg or the infused triax hybrid fabric, is very fatigue resistant under all loading conditions; other infused fabrics have shown reduced compression resistance (10).
3. Delamination resistance under pure and mixed modes is strongly matrix dependent, with epoxies generally providing the most resistance (10). Ply drop delamination at high fatigue cycles occurs at low strains regardless of R-value, position through the thickness or overall laminate thickness. The thickness of material dropped at a single position is an important geometric parameter; improvements have been demonstrated (9,11,14) for treatments of the ply drop edge, including chamfering and pinking.

3. GEC-DIRECTED BSDS-PHASE II PROJECT

3.1 Project Overview Under the SNL-sponsored, GEC-directed Blade System Design Studies (BSDS) Contract, alternative composite materials, manufacturing processes, and structural designs were evaluated for potential benefits for MW-scale blades (15,16). The BSDS-Phase I project partly consisted of trade-off studies to identify alternative materials and manufacturing approaches to support the development of longer and lighter utility-grade blades.

The primary objectives for BSDS-Part II were to perform coupon and sub-structure testing to evaluate material and process combinations with promise for application to MW-scale blades. The Phase II report is currently in final draft (9).

Testing of composite articles was performed at three laboratories: Integrated Technologies (Intec) in Everett, Washington; Montana State University (MSU) in Bozeman; and Wichita State University (WSU). Efforts were made to ensure that the program is complementary with the DOE/MSU Database testing at Montana State University (5).

Composite materials evaluated include carbon fiber in both pre-impregnated and vacuum-assisted resin transfer molding (VARTM) forms. Thin-coupon static testing incorporated a wide range of parameters, such as variation in manufacturer, fiber tow size, fabric architecture, and resin type. A smaller set of these materials and process types was evaluated in thin-coupon fatigue testing, and in ply-drop and ply-transition panels. The majority of materials used epoxy resin; however, vinyl ester (VE) resin was also used for selected cases. Testing of unidirectional fiberglass was added late in the project to provide an updated baseline against which to evaluate the carbon material performance.

Numerous unidirectional carbon fabrics were considered for evaluation with VARTM infusion. All but one fabric style considered suffered either from poor infusibility or waviness of fibers combined with poor compaction. The exception was a triaxial carbon-fiberglass fabric produced by SAERTEX. This fabric became the primary choice for infused articles throughout the test program. The generally positive results obtained in this program for the SAERTEX material have led to its being used in innovative prototype blades of 9-m and 30-m length.

As noted above, obtaining good structural performance with a VARTM process presents significant manufacturing challenges. Figure 5 shows how stitching can adversely affect the straightness of carbon fibers in a unidirectional fabric.

Figure 6 shows the most favorable fabric identified, a multi-layer, multi-axial warp-knit (MMWK) style produced by SAERTEX. GEC worked with the vendor and TPI Composites to develop this architecture. The fabric is a triaxial construction $[-45^{\circ}_{\text{Glass}}/0^{\circ}_{\text{Carbon}}/+45^{\circ}_{\text{Glass}}]$ with areal weights of 150/670/150 gsm. The net fiber content is 75% carbon and 25% fiberglass by volume.

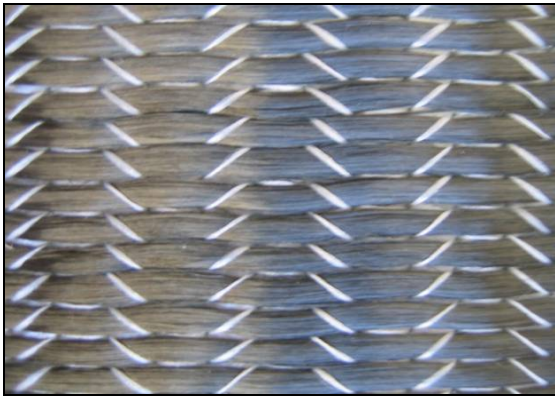


Figure 5: Stitched fabric with manufacturing-induced waviness.

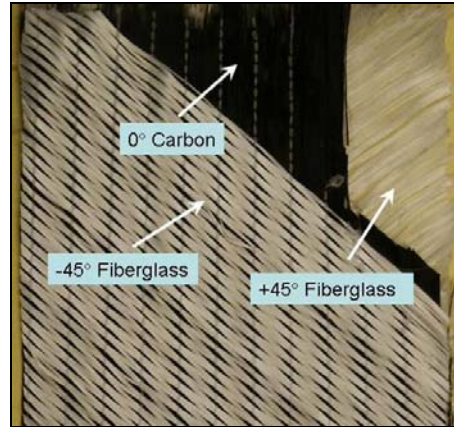


Figure 6: SAERTEX triaxial carbon-fiberglass fabric.

Distinct features of this architecture and SAERTEX stitching style include:

- the outer layers are fiberglass, providing some protection of the carbon fibers;
- the stitching pattern is such that it squeezes the glass strands, but runs parallel with and between strands of carbon fibers;
- the resulting fabric has good infusibility without introducing waviness in the carbon fibers; and
- the triaxial construction provides good stability for material handling.

3.2 Ply Drop Panels To study the effects on ply delaminations due to ply drops in the material, two styles of panels with ply drops were fabricated: drops with standard straight edges and drops with serrated or “pinked” edges as illustrated in Figure 7.

The motivation for fabricating and testing the panels with the pinked ply drops was to reduce the stress concentration at the ply drop edge. Both the straight and pinked configurations were fabricated in prepreg and infused articles. Asymmetries in the ply drop coupons due to manufacturing issues created challenges for obtaining reliable results in compression testing. Therefore, the majority of fatigue testing for the ply drop specimens was performed in tension ($R = 0.1$). Ply drops were tested in both straight and pinked edge geometries. Figure 8 shows results for ply drop panels manufactured at Montana State University (MSU) using Grafil/Newport prepreg material. The data represent the number of cycles required to develop a delamination of 6.35 mm (0.25 inch). As indicated in the figure, for the straight ply drop (control) the strain level for 10^6 cycle delamination is below 0.3%. The fatigue performance for the pinked coupon is greatly improved, with 10^6 strain increased to above 0.5%.

Figure 9 and Figure 10 show results for infused ply drop panels manufactured at TPI using SAERTEX carbon-fiberglass triax fabric with both epoxy and VE resins, in both straight and pinked configurations. The trends for both epoxy and VE resins are quite similar. For the straight-edge configuration, the 10^6 strain is about 0.3%, and only slightly higher for the epoxy resin than for VE. The improvement due to pinking is less than was seen for the prepreg materials, with 10^6 strain values increase to about 0.4% for both epoxy and VE.

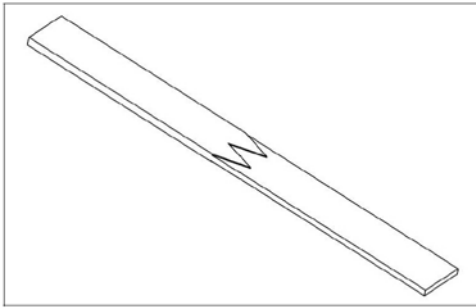


Figure 7: Pinked ply drop specimen geometry.

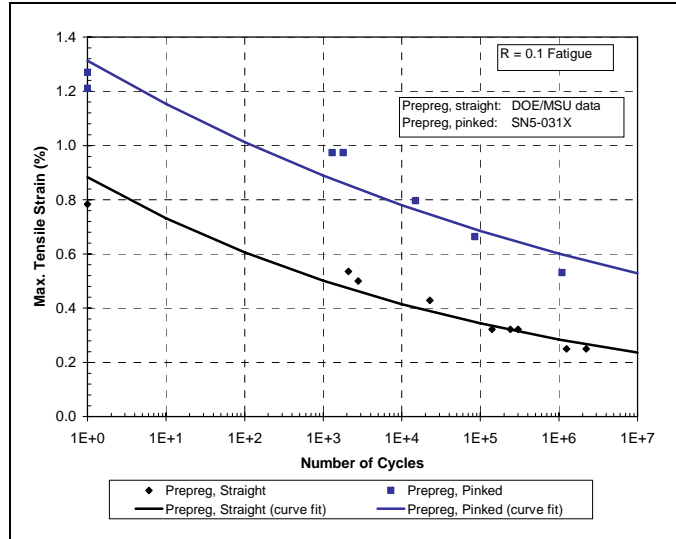


Figure 8: Tensile data for prepreg ply drop specimens.

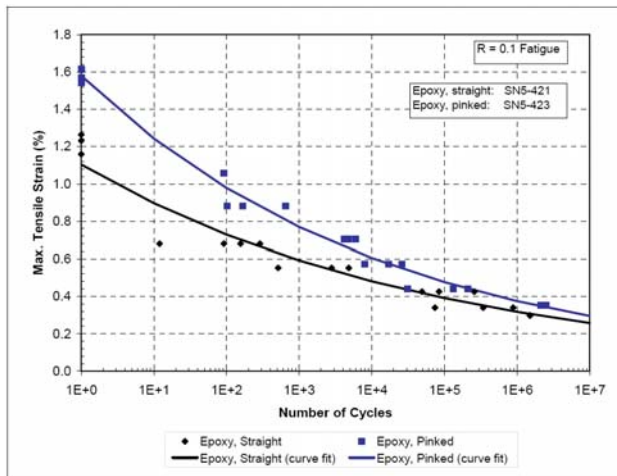


Figure 9: Tensile data for infused epoxy straight and pinked ply drops.

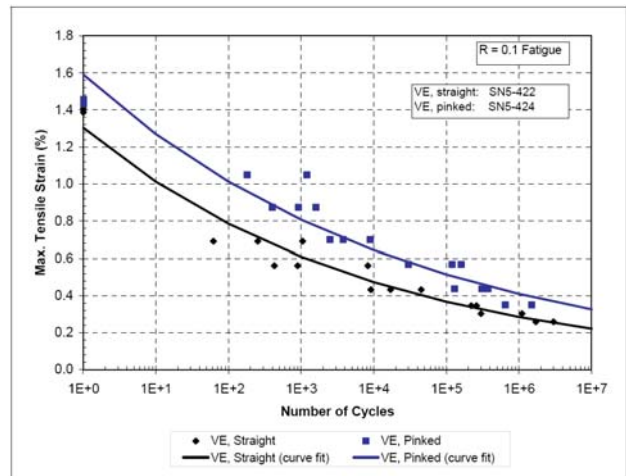


Figure 10: Tensile data for infused VE straight and pinked ply drops.

For all fabric and resin styles, a ply drop with a straight edge resulted in lower fatigue performance than the same fabric and resin with a pinked ply drop. For prepreg laminate, the introduction of a pinked-ply drop edge nearly doubled the strain level for delamination at 10^6 cycles. With the infused fabrics, the pinked edge showed far less benefit, with a strain improvement at 10^6 cycles was only about 25%.

The relatively low fatigue performance for the infused ply drops with pinking may be partly due to the geometry of the ply drops and panels. Carbon fiber is difficult to cut and Figure 11 shows that the accuracy of the pinking in the SAERTEX fabric is far from ideal. By contrast, the tacky nature of prepreg materials makes precise cutting much easier.

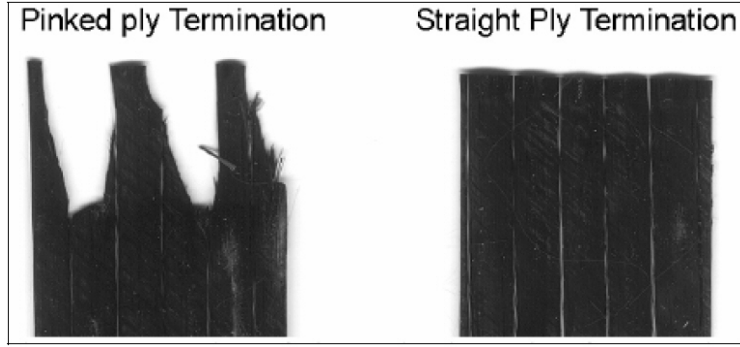


Figure 11: Face view of ply terminations.

3.3 Infused Fiberglass Fatigue Results Figure 12 shows fatigue data ($R = 0.1$ and 10) for the E-LT-5500 fiberglass fabric, infused with both epoxy and VE resins. Strain values in these figures were calculated by GEC based on the MSU-measured stress levels combined with the average modulus measured by Intec in static testing.

The tension ϵ - N curve of Figure 12 shows several trends. For both the epoxy and VE resins, the intersection of the curves at zero cycles is substantially higher than the measured single-cycle strain. At higher cycles, the VE tension fatigue strength falls consistently below that of the epoxy.

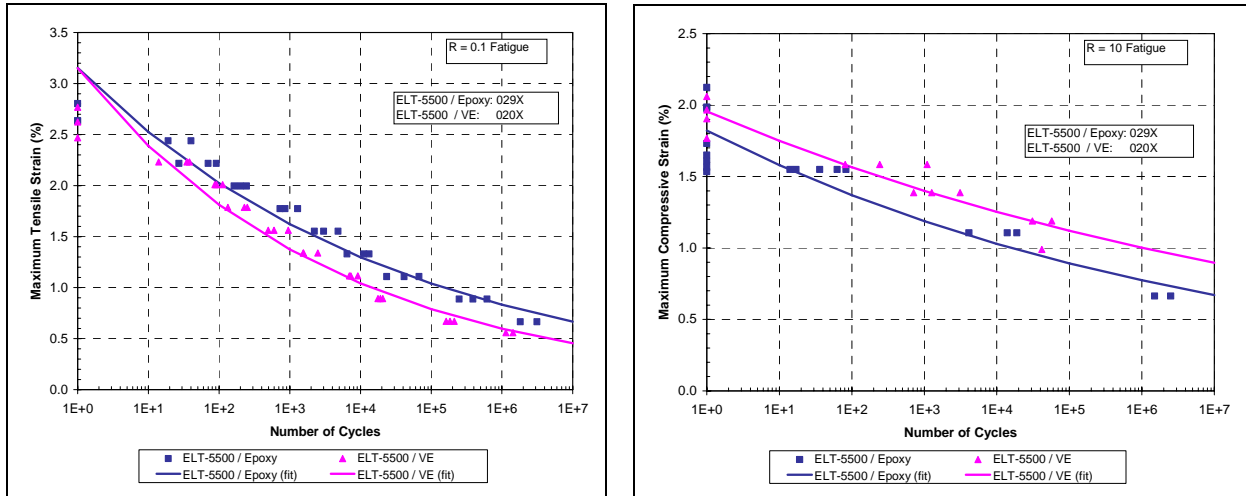


Figure 12: $R = 0.1$ (left) & 10 (right) fatigue data for thin-coupon infused fiberglass.

Significantly different trends are seen in the compressive strain fatigue data. Most notable is that the VE data fall consistently above that of the epoxy. The curves are also flatter than those seen for the $R = 0.1$ data (i.e. they have higher fatigue exponent).

3.4 Prepreg Carbon Fatigue Results Figure 13 shows fatigue data for three styles of carbon prepreg material. The data for the Grafil/Newport material were developed by MSU under the DOE/MSU Database program. Data for Toray and Zoltek fibers (SP WE90-1 resin with PMP) came from testing conducted at MSU under the BSDS-II study.

The data of Figure 13 shows that the Grafil and Zoltek fibers had very similar ϵ -N curves for $R = 0.1$ fatigue. The Toray data showed higher values for single-cycle tension, and a somewhat steeper slope throughout the curve. However all three curves for $R = 0.1$ fatigue were very flat, with slope parameter (m values) ranging from about 31 to 41.

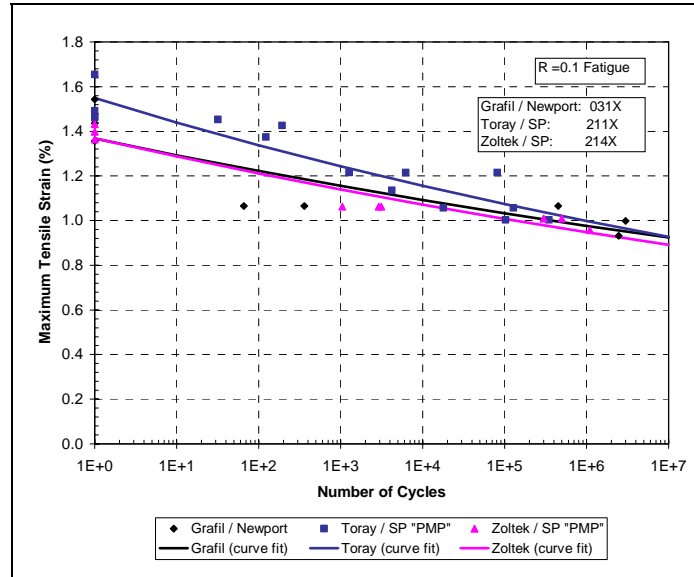


Figure 13: $R = 0.1$ Fatigue data for thin-coupon prepreg panels.

3.5 Infused Carbon Fatigue Results Figure 14 presents fatigue data for the VARTM-infused carbon-fiberglass triaxial fabric. Curve-fit parameters are listed in (9). The test panels include both epoxy and VE resins. It was noted in the above section on static strength testing that although the laminate schedule is identical for these panels, the differential in measured modulus results in different trends for stress and strain comparisons.

In tension ($R = 0.1$), the fatigue performance of VE was clearly lower than epoxy. The single-cycle stress for the infused VE material was slightly higher than that for the epoxy, but at a million cycles was about 25% lower. In compression ($R = 10$) loading, the VE stress levels were consistently higher than the epoxy, with a differential of about 5% at low cycles, growing to more than 10% at high cycles. As expected, applying the higher compressive modulus in the VE strain calculations resulted in a shift between the curves. Calculated VE strains for $R = 10$ fatigue are about 7% lower than epoxy at low cycles, and 2% lower at high cycles (see reference 9 for further explanation).

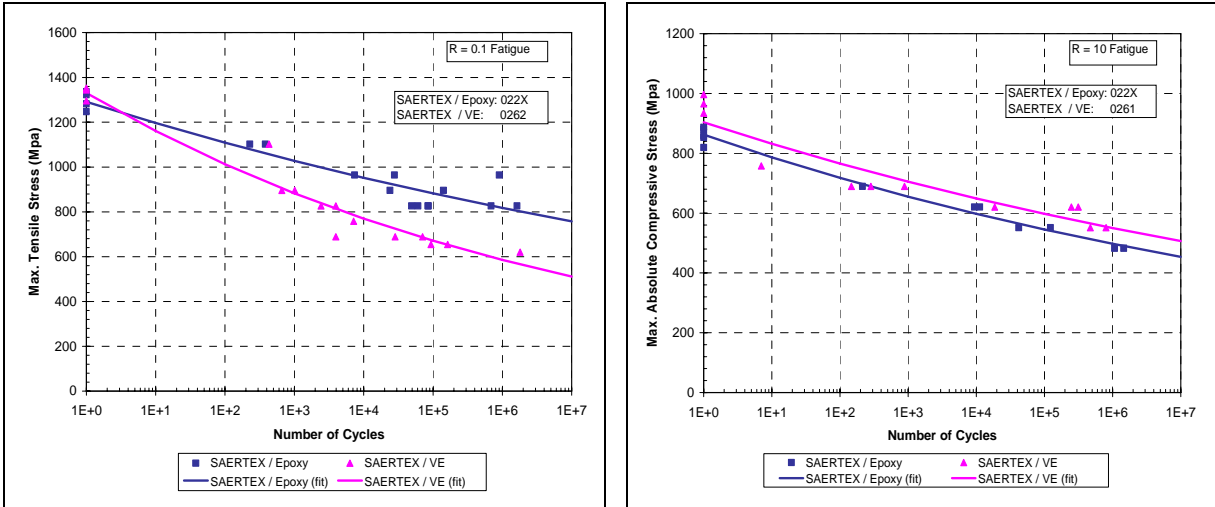


Figure 14: R = 0.1 & 10 fatigue data for VARTM infused carbon-fiberglass triaxial fabric.

3.6 Comparison of Fatigue Data for Prepreg and Infused Carbon Panels Figure 15 shows comparisons of fatigue data for prepreg and infused (epoxy) carbon panels. The infused panels use the SAERTEX carbon-fiberglass triaxial fabric with a substantial amount of integral $\pm 45^\circ$ fiberglass fibers, whereas the prepreg panels are primarily unidirectional carbon tape, with a small amount of $\pm 45^\circ$ glass in the facings. Consequently, the modulus of the infused panels is by design lower than the prepreg materials. In terms of evaluating the performance of the carbon fibers in the laminate, a comparison of strain levels provides a more valid basis than does the stress.

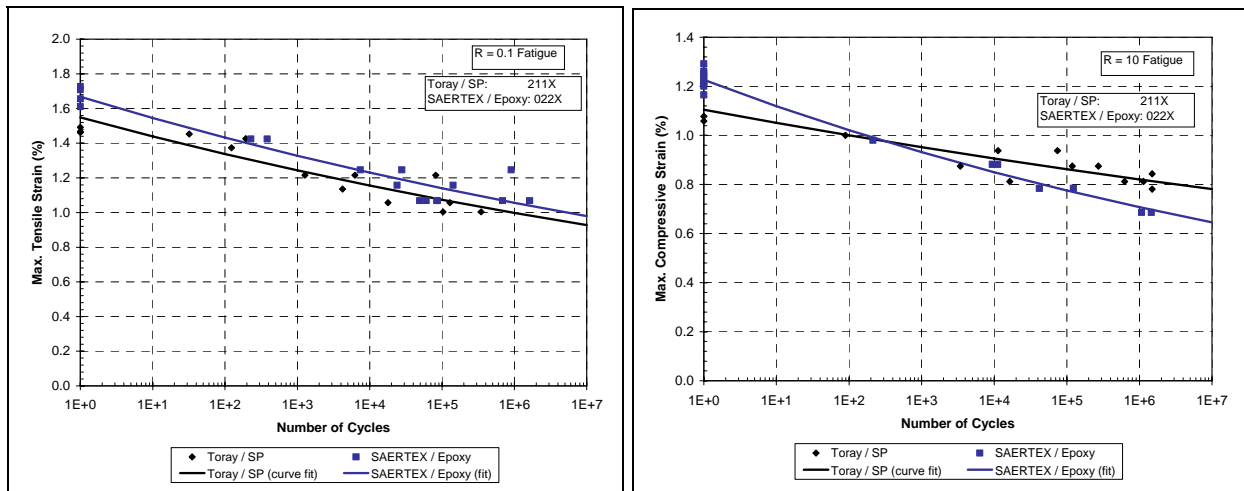


Figure 15: R = 0.1 & 10 fatigue data for prepreg and infused (epoxy) panels

The R = 0.1 data for Toray prepreg and epoxy-infused triax panels indicates that the overall performance for these materials is quite similar. Strain values for the infused article are modestly higher than those for the prepreg over the entire range of cycles. A somewhat different trend exists for the R = 10 fatigue. At the single-cycle end of the ϵ -N curve, the infused triax panel strains are about 10% higher than the prepreg, but at 10^6 cycles, the triax strains fall below the

prepreg by 20%. The $R = 10$ slope is steeper for the infused material. The prepreg ϵ - N curve has a slope parameter of $m \approx 46$, whereas the triax has an $m \approx 25$. Comparisons for $R = -1$ (fully reversed fatigue) loading (9) show very close agreement between the infused material and the Toray prepreg.

3.7 Observations and Conclusions for GEC-BSDS Phase II Testing A range of carbon fiber styles and tow sizes were tested in prepreg form and generally found to have little variation in performance.

Numerous unidirectional carbon fabrics were considered for evaluation with VARTM infusion. Most fabric styles considered suffered either from poor infusibility or waviness of fibers combined with poor compaction. The exception was a triaxial carbon-fiberglass fabric produced by SAERTEX. This fabric became the primary choice for infused articles throughout the test program. The generally positive results obtained in this program for the SAERTEX material have led to its being used in innovative prototype blades of 9-m (17,18) and 30-m (19) length.

Infused articles were tested with both epoxy and VE resin systems. Comparisons between prepreg and infused epoxy, and between infused epoxy and VE were somewhat complex. In some cases, the performance variations were minimal and in other instances they were quite significant. For complex articles (ply drops and ply transitions), the comparison between prepreg and VARTM articles was complicated by the relative lack of symmetry in the infused articles.

3.7.1 Thin Coupon Static

3.7.1.1 Carbon Fiber Thin-coupon testing of prepreg materials showed little variation in static strength with manufacturer or tow size. Average values for compressive static strain were typically in the range of 1.0%-1.1%. The SAERTEX carbon-fiberglass triaxial fabric with epoxy infusion achieved static strain values similar to prepreg materials. However, because of the inclusion of the $\pm 45^\circ$ glass, the modulus and stress at failure are both lower than for the unidirectional carbon prepreg, however, the carbon fibers in the infused laminate are reaching performance levels comparable to that of a unidirectional prepreg. With VE infusion, the SAERTEX triaxial materials achieved slightly higher compressive static strength than that of the epoxy-infused articles. Large differences in measured compressive modulus would not be expected. In general, the stress measurement (which is based on applied load) is more reliable than the compressive modulus measurement (which is based on a strain gage on a small specimen).

3.7.1.2 Fiberglass Static testing was performed for the E-LT-5500 fiberglass fabric, infused with both epoxy and VE resin. In general, the fiberglass material showed good performance in static strength for both epoxy and VE. Average tensile strain approached 2.3% for both resin systems, with very low coefficients of variation ($COV \leq 2\%$). Average compressive strains were only slightly lower at approximately 2.2%.

3.7.2 Thin-Coupon Fatigue

3.7.2.1 Carbon Fiber Two styles of carbon fiber were tested in a prepreg form: Toray T600 (24k) and Zoltek Panex 35. Each of these fibers was impregnated by SP Systems, using their

WE90-1 resin and PMP process. A third data set was provided by MSU for comparative purposes, fabricated from Grafil 34-600 fibers (48k) and Newport NB307 resin. For all three prepreg materials, thin-coupon fatigue testing was performed at $R = 0.1$, 10 and -1 . In general, the three prepreg carbon materials showed very similar fatigue performance. No consistent trend was seen concerning tow size.

Epoxy-infused (SAERTEX triax) fabric performed fairly well in fatigue relative to the prepreg materials for all R values tested ($R = 0.1$, -1.0 and 10). For the infused carbon panels in tension ($R = 0.1$), the fatigue performance of VE was generally lower than epoxy. The single-cycle stress for the infused VE material was slightly higher than for the epoxy, but was about 25% lower at a million cycles. In the fatigue stress data for compression and reversed loading, there are significantly different trends seen between the VE and epoxy results. In $R = 10$ loading, the VE stress levels were consistently higher than the epoxy, with a differential of about 5% at low cycles, growing to more than 10% at high cycles. Fatigue data for $R = -1$ are relatively sparse and show only modest difference in measured stress between epoxy and VE. The VE curve is steeper than that for epoxy, partly due to higher values of single-cycle stress. As noted above, applying the measured compressive modulus values to these curves would result in a downward shift of the calculated VE strains relative to the epoxy. Because the static testing at Intec had measured higher modulus values for the infused VE panels than for the epoxy, a strain-based compression tends to shift all the VE curves downward relative to the epoxy data.

3.7.2.2 Fiberglass Fatigue testing was also performed for the E-LT-5500 fiberglass fabric, infused with both epoxy and VE resin. In both tension and compression, the single-cycle strain values showed modest variation between the epoxy and VE resins. The single-cycle tensile strain was higher than the static value measured at Intec, and the compressive single-cycle strains were lower than the corresponding static measurements.

3.7.3 Carbon Ply Drop Asymmetries in ply drop and ply transition panels created challenges for obtaining reliable results in compression testing. Therefore, the majority of fatigue testing was performed for $R = 0.1$. Similar trends could be expected for $R = 10$, and $R = -1$, with an overall reduction in the fatigue performance expected. In performing the ply-drop tests, “failure” was determined by the number of cycles require to develop a delamination of 6.35 mm.

Ply drops with a straight edge for all fabric and resin styles resulted in low fatigue performance. The introduction of a pinked-ply drop edge almost doubled the strain level for delamination at 10^6 cycles for the prepreg laminate. With infused fabrics, the pinked edge showed far less benefit, with a strain improvement at 10^6 cycles of only about 25%.

The relatively low fatigue performance for the infused ply drops with pinking may be partly due to the geometry of the ply drops and panels. Visual inspection after resin burn-off showed that the shape of the “pinked” fabric was significantly better for the prepreg than for the infused articles. MSU also noted the contribution of through-the-thickness asymmetry to the failure mode of the infused ply-drop articles.

3.7.4 Carbon-Fiberglass Ply Transition Ply-transition panels were fabricated in two bounding cases for the carbon-to-glass transition of a structural spar: 1.) mostly carbon, in which the article might represent the first carbon ply being transitioned to fiberglass in a carbon spar cap and 2)

mostly fiberglass which represents the last carbon ply being transitioned. These two arrangements were considered as the bounding cases. Both of these configurations were fabricated in prepreg and infused articles.

Initial ply-transition panels infused by TPI using the SAERTEX carbon-glass triaxial fabric showed unexpectedly poor performance in tensile strength, with delaminations initiating at relatively low strain values. The early delamination was attributed primarily to asymmetry in the thickness taper and the placement of fiberglass doublers at the outer-most location in the stack of unidirectional plies.

Based on the lessons learned from the initial infused articles, the transition panels were redesigned and fabricated at MSU using Grafil/Newport prepreg material. In an attempt to delay the onset of delamination, the fiberglass doublers were moved to the interior of the unidirectional fabric stack.

R = 0.1 testing of the second-iteration prepreg panels, completed at MSU, shows a significant reduction in fatigue performance in going from one to two ply transitions (mostly glass data). However, the tensile strain values for delamination at 10^6 cycles are close to 0.5%, which compares somewhat favorably with results for the ply-drop coupons.

Testing at MSU is continuing for prepreg transition panels in compression, and for second-iteration epoxy-infused ply-transition panels at R = 0.1, 10, and -1. Results from these tests will be reported by MSU as part of the ongoing development of the DOE/MSU Database.

4. PROTOTYPE TESTING

4.1 Introduction In 2002 SNL initiated a research program (20) to demonstrate the use of carbon fiber in subscale blades (21) and to investigate innovative concepts through the BSDS projects (22-24). From this effort, three 9 m designs were created by SNL with assistance from GEC, Dynamic Design Engineering, and MDZ Consulting; and seven blades from each design were manufactured by TPI Composites. All blades were designed for a 100 kW stall controlled turbine. The first blade set was called CX-100 (Carbon Experimental), and contained a full-length carbon spar cap, a relatively new concept at the time. The geometry of the CX-100 was based on the design of the ERS-100 (25) blade at outboard span stations, and the Northern Power Systems NW-100 blade in the root area. The second blade design, the TX-100 (Twist-Bend Experimental), had the same geometry as the CX-100, but was designed to have passive aerodynamic load reduction by orienting unidirectional carbon 20° off of the pitch axis in the skins from approximately 25% span outward. Studies (26-31) had indicated the possibility of such a method of passive aerodynamic load alleviation through material induced twist-bend coupling, with 20° being determined as the optimum angle. The TX-100 also contained a fiberglass spar cap which terminated at the mid-span of the blade. The third blade design was termed the BSDS (Blade System Design Studies), the name of the research solicitation under which it was created. The BSDS has a length of 8.325 m rather than the 9.000 m length of the CX-100 and TX-100. This blade design included features as a thin, large-diameter root; flatback airfoils; integrated root studs; and a full-length, constant-thickness, and carbon spar cap.

A drawing of these blades is shown in Figure 16 with the carbon areas shown in blue. Note the carbon spar caps of the CX-100 and the BSDS blades, and the carbon outboard skins of the TX-100. The unidirectional fiberglass spar cap of the TX-100 is shown in red and extends only to the mid-span of the blade. It was determined that the large amount of carbon contained in the skin was adequate to carry loads outboard in this design, making a full length spar cap unnecessary. The narrow, constant thickness spar cap of the BSDS blade alludes to the inherent structural stiffness of this design. In addition, the BSDS design features a gradual transition between the root and max-chord areas as compared to the CX and TX plan form.

Figure 17 shows the airfoil geometries and relative sizes at the root, max-chord, and tip of the CX-100, TX-100, and BSDS blades. The BSDS blade can be seen to have a larger root diameter while also having a shorter max-chord length. The tip airfoil of the BSDS blade is representative of the outboard airfoils, which are thin and aerodynamically high performing.

A suite of laboratory and field tests are verifying the extent to which the manufactured blades meet their design goals. To date, specimens from each design have undergone modal, static (35) and fatigue testing (36).

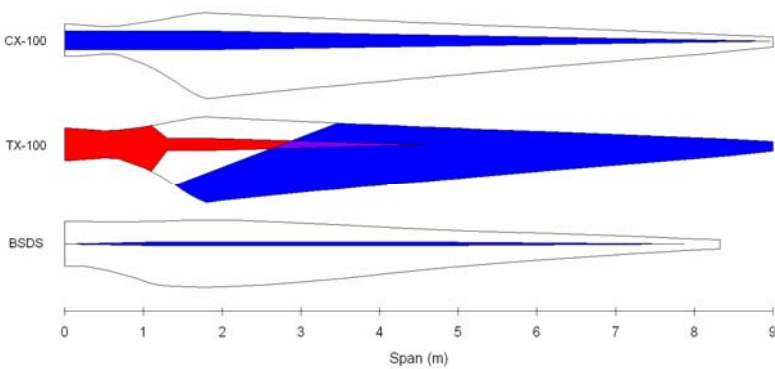


Figure 16: 9 m Blade Plan Form and Major Material Regions

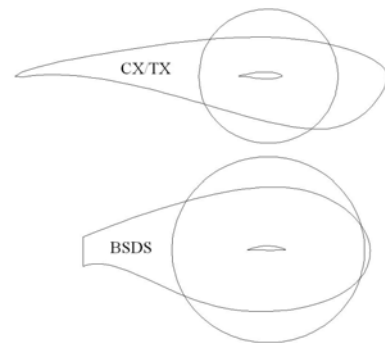


Figure 17: 9 m airfoil geometries at root, max-chord, and tip.

4.2 Static Test Setup One blade from each design set was statically tested to failure at the National Wind Technology Center (NWTC) near Boulder, CO. The blades were mounted to a 1360 kN-m test stand and subjected to a flapwise bending load case to approximate the extreme loading events for the wind class to which each blade was designed (32). The extreme load case resulted in a root moment of 86.4 kN-m for the CX-100 blade and in a root moment of 53.8 kN-m for the TX-100 and BSDS blades. All blades were loaded by use of a three-point whiffle tree and saddle arrangement connected to an overhead bridge crane which is shown schematically in Figure 18.

For the TX-100 blade test, a rope and pulley arrangement was attached to the saddles in an attempt to allow twisting without altering the loading point. The blades were loaded and unloaded in increasing 25% increments up to the 100% test load. Also, an array of sensors was used in the tests to monitor strain, deflection, load, and acoustic emissions. All three blade designs successfully withstood the prescribed test loads. Deflections, rotations, and strain were

measured. The spar cap strains measured near failure are shown in Figure 19. In the case of the TX-100 blade, the spar cap terminates at the mid-span of the blade and thus strains outboard of that point are along the blade centerline. The carbon spar cap of the CX-100 blade experienced strains of around $3000 \mu\epsilon$ before failure. The TX-100 blade exhibited maximum strains of approximately $5500 \mu\epsilon$ near the termination point of the spar cap and strains elsewhere in the blade were generally lower. The high strain at the spar cap termination was likely the result of a stress concentration emanating from the tapered end of the spar cap. The carbon spar cap of the BSDS blade experienced maximum strains of over $8000 \mu\epsilon$ on both the high-pressure and low-pressure surfaces.

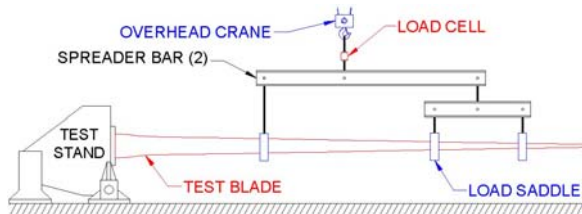


Figure 18: Three point whiffle-tree used in 9 m static blade tests.

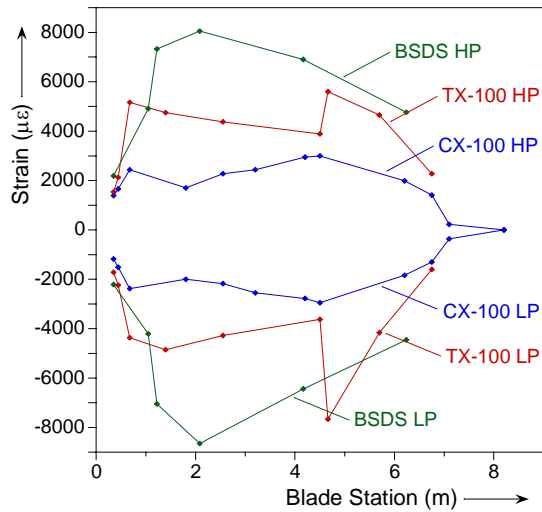


Figure 19: 9 m spar cap strains near failure

Acoustic emissions sensed by microphones placed on the blade surface can be used to indicate the location of damage that incurred in the blade during testing. An example the use of this technology is shown in Figure 20 for the CX-100 where measured acoustic events are overlaid on an outline of the blade. Each event is color coded with a relative energy range, which represents the integral of the voltage vs. time curve. Although not the true energy, these voltage vs. time results are useful for comparative purposes. During the CX-100 test, several high-energy events were located between 1.20 m and 1.30 m along the spar cap. The CX-100 blade was observed during failure to experience a catastrophic buckling of the low-pressure skin near the 1.2-m station. A post mortem inspection of the blade in this region did indeed show a large crack in the bond joint between the low pressure skin and the shear web.

A summary of results of the static tests of all three blade designs is contained in Table 1. The relatively high strength of the BSDS blade is evident, with the measured carbon strains approaching values seen in coupon testing of pre-preg specimens. This high strength combined with the significantly lower weight points to the structural advantages of this design in comparison to the CX-100 and TX-100, which were both significantly better performers than the baseline ERS-100.

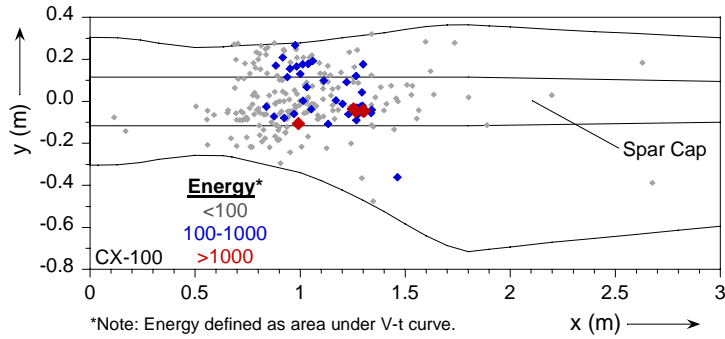


Figure 20: Acoustic event locations and energies for CX-100.

Table 1: Summary of results of 9 m blade tests.

| Property | CX-100 | TX-100 | BSDS |
|---|--------|--------|-------|
| Weight (lb) | 383 | 361 | 289 |
| % of Design Load at Failure | 115% | 197% | 310% |
| Root Failure Moment (kN-m) | 128.6 | 121.4 | 203.9 |
| Max. Carbon Tensile Strain at Failure (%) | 0.31% | 0.59% | 0.81% |
| Max. Carbon Compressive Strain at Failure (%) | 0.30% | 0.73% | 0.87% |
| Maximum Tip Displacement (m) | 1.05 | 1.80 | 2.79 |

4.3 Summary of Static Testing Specimens from three 9-m carbon fiber blade designs underwent static structural testing. All three test blades survived factored design test loading. The CX-100 blade displayed exceptional stiffness, deflecting only 1.05 m at a root moment of 128.6 kN-m. The blade failed due to panel buckling near max-chord which was likely initiated by a separation between the shear web and the low-pressure skin in that region. The TX-100 blade successfully demonstrated twist-bend coupling caused by 20°-off-axis carbon in the outboard skins. The TX-100 blade failed at a slightly lower load than the CX-100 blade, but in a similar location. The BSDS blade displayed exceptional strength in comparison to the CX-100 and TX-100 designs, surviving to almost three times the target test load. The flatback airfoil feature performed well and did not display non-linear behavior until well after the target test load was reached. In addition, the root mounting studs of the BSDS blade were observed to have good static loading properties. Finally, the acoustic emission monitoring system detected not only the locations where damage was occurring, but also incipient global blade failure.

4.4 Fatigue Test Setup The CX-100 and TX-100 blades were tested at the National Wind Technology Center (NWTC) near Boulder, CO.

4.4.1 CX-100 A decision was made early in the test planning to load the CX-100 blade by means of a hydraulic cylinder located at the 5600-mm station of the blade. Single-point hydraulic loading has the benefit of being a simple and robust way to fatigue load a blade, but this comes at the expense of not being able to match the desired loading distribution as well as with other loading methods. An R-ratio of 0.1 on the high-pressure surface of the blade was desired in order to simulate operational conditions.

Fatigue test loading distributions were calculated to determine cyclic resonate distributions for sets of equivalent fatigue lives. Those calculations take into account the proper fatigue slope,

material safety factors and simulation of turbine operations. A fatigue slope of 12 was chosen as a compromise between the value of 10 used for fiberglass and 14 used for carbon composites.

There were two principal factors in the design of the fatigue test. First, the test needed to demonstrate an equivalent 20-year operation life. Second, the test needed to be completed in a reasonable cycle count (i.e. 1-4 million cycles).

The CX-100 was conducted as a single-axis, flapwise forced displacement test. A hydraulic actuator was affixed to the blade at the 5700-m station. The actuator line-of-action was through the blade axis. A control frequency of 1.3-Hz was used to apply test loads. During the fatigue test displacement, control of the actuator was employed for test stability. The target moment distributions are shown in Figure 21.

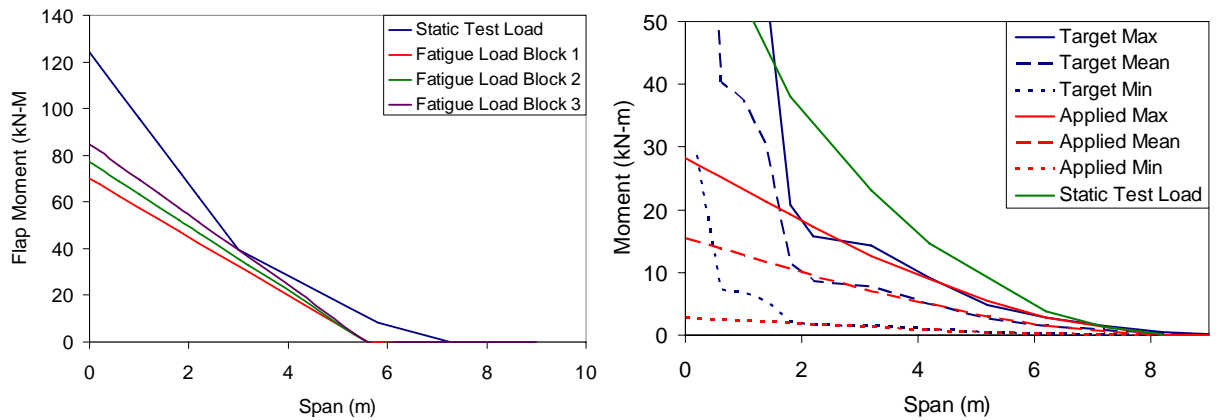


Figure 21: CX-100 and TX-100 fatigue peak loading targets.

4.4.2 TX-100 The fatigue load for the TX-100 blade was analyzed similarly to that of the CX-100 blade. A slope coefficient of 12 was used instead of 14 to account for the flap loads being oriented at 20° from the carbon fiber direction. In addition, the blade was to be loaded via a resonant loading method that allowed the target loading to be better approximated along the blade span and did not restrict the twist dynamics of the blade. Like for the CX-100, rainflow counts of load cycles acquired from system dynamics simulations were used to compute 20-year damage fractions.

Test loading targets were developed from the damage analysis. Similar to the CX-100 test, the loads were partially driven by the desire for a test of reasonable duration. Also like the CX-100, it was decided that the load would be increased in increments of 10% every 0.5 million cycles starting at the 1 million cycle count. To serve as a guide, fatigue test loading distribution for 1, 2, and 4 million cycle tests were developed. These load distributions are shown in Figure 21, along with the moment distribution from an earlier static test of another TX-100 blade. The load step increase schedule would show a 20-year life at the 2 million cycle count.

A resonant test apparatus (33) was used to conduct the TX-100 fatigue test. The test was configured as a single-axis flapwise resonant test, which was conducted by affixing a resonant mass and ballast saddles to the cantilevered test article. Hydraulic actuators controlled the resonant mass. By exciting the resonant mass at the natural frequency of the system, an

alternating test bending moment was applied to the blade. The location and weight of the excitation mass and ballast saddles prescribed both the mean load and the characteristic shape (mode shape) of the alternating moment. The weight and actuated distance of the resonant mass controlled the amplitude of the alternating test load.

A novel resonant test apparatus was developed at NREL for this test. The UREX (Universal Resonant EXciter) was used to apply the test loading. The UREX was developed specifically for the unique aspects of testing bend-twist coupled blades. The UREX uses a pair of hydraulic actuators mounted to the blade through a ballast saddle. The actuators are located on each side of the blade (see Figure 22).

This sidesaddle arrangement has advantages over previous single-actuator designs. The primary advantage of the UREX is that the rotational inertia is minimized in comparison to mounting the actuator and resonant mass above the center of the blade, which could impart undesired torsional loading, thus distorting the bend-twist response of the test article. Figure 23 provides a photograph of the TX-100 test setup. In addition, although not employed for the TX-100 test, the UREX can tune an applied torsional loading by adjusting the displacements, relative phases, and associated oscillating masses for the two independent actuators.

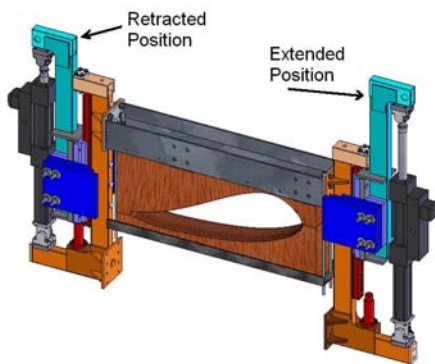


Figure 22: UREX Schematic.



Figure 23: TX-100 Test setup photograph.

The UREX system was located at the 1600-mm station, with a ballast saddle at the 6750-mm station. The UREX system and ballast saddles were located in spanwise areas away from critical structural regions of the blade. (Locations and ballast masses were optimized by using resonant test codes developed at NREL to apply a test bending moment to match the target test load and maintain the r-ratio of 0.1). Figure 21 shows the ability of the UREX to match the loading targets.

The TX-100 blade was outfitted with several data acquisition and structural health monitoring systems. The baseline data acquisition system used to monitor the test was composed of 30-strain gages. Strain, load, and displacement were monitored and recorded for the duration of the test as peak-valley pairs.

4.5 Fatigue Test Results and Analysis After each test, the data were analyzed and a postmortem inspection performed on the blades. The data were reduced by block averaging data points, 1000 points per block. The general strategy was to look at measures of overall damage compared to local areas.

4.5.1 CX-100 Results from strain gauges located in the aft panel near max-chord are shown in Figure 24. Gages 19 and 20 show a marked change beginning shortly after 1.25 million cycles. The change in these measurements is seen to be up to 30%.

The CX-100 test proceeded without significant damage until the 1.5-million cycle count. Spanwise surface cracks were noted at the 1.5-million cycle count between the 1200-mm and 1400-mm stations. These surface cracks formed at the junction of the carbon spar cap and the trailing edge panel. By the 1.6-million cycle level, the cracks had progressed through the thickness of the skin and the test was stopped. In addition, the blade stiffness had decreased by approximately 12% from the initial stiffness, and the lead-lag motion of the blade progressively increased. Subsequent investigations indicate that the increased crack length and development of a disbonding between the LP skin and spar cap led to an increasingly larger out of plane panel deformation leading to gross panel buckling. Figure 25 provides a photograph of the damage area of the CX-100.

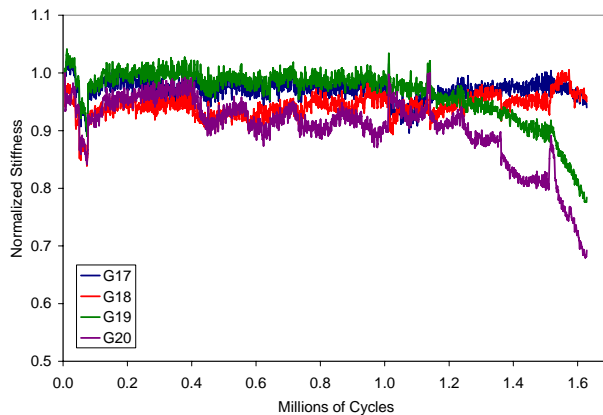


Figure 24: Normalized stiffness at CX-100 strain gages 17, 18, 19, and 20.

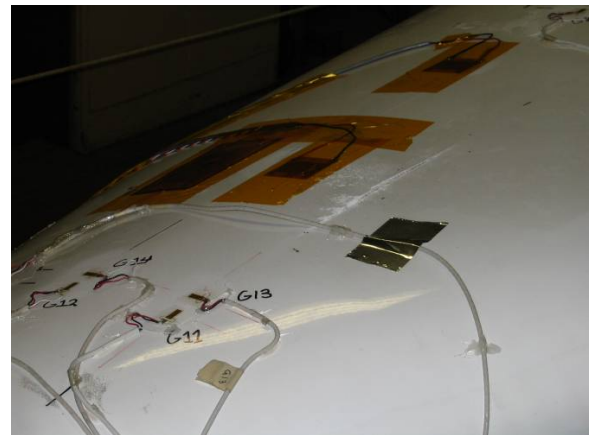


Figure 25: CX-100 low-pressure skin damage area.

4.5.2 TX-100 Multiple sensors were mounted on this blade as the TX-100 served as a test bed for structural health monitoring sensors (34).

Strain gage results were examined to look for signs of damage. A gage mounted just outboard of the tip of the glass spar cap shows that this area began to experience softening before 1 million cycles and gradually progressed throughout the test (Figure 26). The blade eventually failed due to a crack which appeared just outboard of the spar cap on the high pressure surface. The crack initially grew along the axis of the glass layers in the carbon/glass triax material before changing direction to run along the carbon fiber axis. A photo of the failure area is shown in Figure 27.

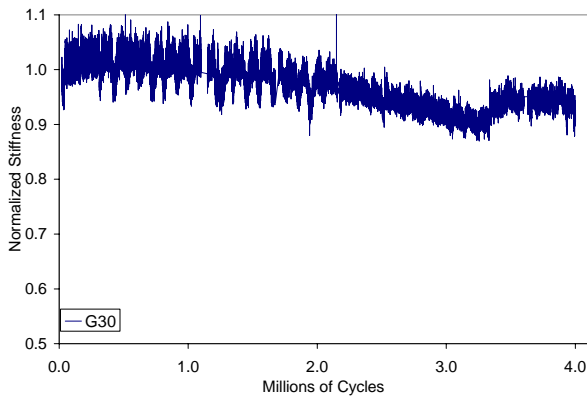


Figure 26: Normalized load/strain of TX-100 at strain gage 30.



Figure 27: TX-100 high-pressure skin damage area.

4.5.3 Summary of Fatigue Tests Both the CX-100 and TX-100 blades demonstrated 20-year equivalent fatigue test loads. The CX-100 needed to complete only 6,000 cycles at its initial load level to demonstrate adequate fatigue resistance but survived past 1.6 million cycles. The TX-100 design was a less stiff design and needed to survive to 2.0 million cycles under the load step regime. The blade failed at over 4 million cycles. While further validation of the blade designs through field testing is planned, the laboratory tests provide a favorable result for hybrid glass/carbon designs. The CX-100 incurred incipient damage above the target fatigue test load. The epicenter of the damage was at the interface of the carbon spar cap and glass/balsa panels, an interface between two laminates with greatly differing stiffness. The TX-100 also maintained structural integrity (stiffness) past the design fatigue life but grew a severe crack along the carbon fiber line beginning at the sharp termination of the spar cap. Thus, while both blades withstood the required number of cycles to demonstrate a 20-year operational life, the unique design aspects of both blades played a role in their eventual failure. Also of importance was that while the fatigue calculations were based on fiber direction material properties, the off direction material properties played a role in the eventual failure of both blades. This demonstrates the difficulty in incorporating innovative design features in a fatigue sensitive structure and the difficulty of performing accurate fatigue life predictions based on limited material property data and simple models.

SUMMARY

This paper provides an overview of recent studies of composite laminates for wind turbine blade construction and summarizes test results for three prototype blades that incorporate a variety of structural and material innovations. Section 2 summarizes recent SNL-sponsored material fatigue testing performed at Montana State University. Section 3 provides highlights of the SNL/GEC Blade System Design Study-Phase II research contract that tested a variety of carbon and carbon-hybrid materials. Section 4 provides an overview of ongoing testing activities in the SNL 9-m prototype research program. Through this work, the value of incorporating carbon into wind turbine blades has been demonstrated. While cost remains a challenge for the implementation of carbon in commercial designs, the work shown and referenced in this paper describes methodologies to produce blades with carbon at much lower costs than that expected with a simple transition of aerospace type manufacturing materials and methods.

ACKNOWLEDGEMENTS

This paper discusses several ongoing SNL directed projects and has borrowed liberally (as noted) from several specific papers that have been or are in the process of being published. Significant contributions are from many and we apologize to those we inadvertently left out.

Montana State University: John Mandell and Dan Samborsky.
GEC: Dayton Griffin and Tim McCoy.
TPI: Derek Berry
MDZ: Mike Zuteck
Dynamic Design: Kevin Jackson
UC Davis: Case van Dam
NREL: Scott Hughes, Mike Jenks, and Jeroen van Dam
Sandia Labs: Daniel Laird, Wesley Johnson, Mark Rumsey

REFERENCES

1. BTM Consult ApS, *World Market Update 2006, Forecast 2007-2011*, Ringkobing, Denmark, March 2006.
2. Ashwill, T, and Laird, D, "Concepts to Facilitate Very Large Blades," *Proceedings, ASME/AIAA Wind Energy Symposium*, Reno, NV, 2007.
3. Ashwill, T.D., "Developments in Large Blades for Lower Cost Wind Turbines", AWEA 2004, Chicago, Illinois.
4. TPI Composites, *Innovative Design Approaches for Large Wind Turbine Blades; Final Report*, SAND2004-0074, Sandia National Laboratories, Albuquerque, NM, 2004.
5. J. F. Mandell and D. D. Samborsky, *DOE/MSU Composite Material Fatigue Database: Test Methods, Materials, and Analysis*, Contractor Report SAND97-3002, Sandia National Laboratories, Albuquerque, NM, 1997.
6. J. F. Mandell and D. D. Samborsky, "DOE/MSU Fatigue of Composite Materials Database. 2007 Update," (<http://www.sandia.gov/wind/other/973002upd0306.pdf>)
7. J. F. Mandell, D. D. Samborsky and P. Agastra, "Composite Materials Fatigue Issues in Wind Turbine Blade Construction," SAMPE 2008, Los Angeles, CA.
8. D. D. Samborsky, P. Agastra and J. F. Mandell, "Effects of Glass Fabric and Laminate Construction on the Fatigue of Resin Infused Blade Materials, *Proc. 2008 ASME Wind Energy Symposium*, ASME/AIAA, Reno, NV, 2008.
9. Griffin, D.A. and Roberts, D., *Blade System Design Studies Volume II: Final Project Report (draft)*, Sandia National Laboratories, Albuquerque, NM.
10. J. F. Mandell, D. D. Samborsky, and D. S. Cairns, *Fatigue of Composite Materials and Substructures for Wind Turbine Blades*, Contractor Report SAND2002-0771, Sandia National Laboratories, Albuquerque, NM, 2002.
11. Wilson, T.J., "Modeling of In-Plane and Interlaminar Fatigue Behavior of Glass and Carbon Fiber Composite Materials," MS Thesis, Department of Mechanical Engineering, Montana State University, 2006.
12. J. F. Mandell, D. D. Samborsky, and L. Wang, *SAMPE International Symposium*, 48, 2653, 2003.

13. Samborsky, D. D., Wilson, T. J. and Mandell, J. F., *Proc. 2007 ASME Wind Energy Symposium*, Paper AIAA-07-67056, AIAA/ASME, Reno, NV, 2007.
14. D. D. Samborsky, D. P. Avery, P. Agastra, and J. F. Mandell, *Proc 2006 ASME Wind Energy Symposium*, Paper AIAA-2006-1195, AIAA/ASME, Reno, NV, 2006.
15. Griffin, D.A., *Blade System Design Studies Volume I: Composite Technologies for Large Wind Turbine Blades*. SAND2002-1879, Sandia National Laboratories, Albuquerque, NM.
16. Griffin, D.A., *Blade System Design Studies Volume II: Preliminary Blade Designs and Recommended Test Matrix*. SAND2004-0073, Sandia National Laboratories, Albuquerque, NM.
17. Berry, D., "Wind Turbine Blades: Blade Manufacturing and Materials Development," Presented at the 2006 Sandia Blade Workshop, Sandia National Laboratories, Albuquerque, NM.
18. Paquette, J., "Lab Testing of Subscale 9m Blades," Presented at the 2006 Sandia Blade Workshop, Sandia National Laboratories, Albuquerque, NM.
19. Griffin, D.A., "Demonstration of an Infused Carbon Fiber Spar in a MW-Scale Blade," Presented at the 2006 Sandia Blade Workshop, Sandia National Laboratories, Albuquerque, NM.
20. Ashwill, T, and Laird, D, "Concepts to Facilitate Very Large Blades," *Proceedings, ASME/AIAA Wind Energy Symposium*, Reno, NV, 2007.
21. C.-H. Ong and S. W. Tsai, *The Use of Carbon Fibers in Wind Turbine Blade Design: A SERI-8 Blade Example*, SAND2000-0478, Sandia National Laboratories Contractor Report, Albuquerque, NM, March 2000.
22. Berry, Derek and Lockard, S., *Innovative Design Approaches for Large Wind Turbine Blades*, SAND2003-0723, Sandia National Laboratories, Albuquerque, NM, March 2003
23. Berry, Derek and Lockard, S., *Innovative Design Approaches for Large Wind Turbine Blades Final Report*, SAND2004-0074, Sandia National Laboratories, Albuquerque, NM, May 2004
24. Griffin, Dayton A., *Blade System Design Studies Volume II: Preliminary Blade Designs and Recommended Test Matrix*, SAND2004-0073, Sandia National Laboratories, Albuquerque, NM, June 2004
25. TPI Composites, Inc., *Blade Manufacturing Improvements: Development of the ERS-100 Blade*, SAND2001-1381, Sandia National Laboratories, Albuquerque, NM, May 2001.
26. P. S. Veers, G. Bir and D. W. Lobitz, "Aeroelastic Tailoring in Wind-Turbine Blade Applications," *Proceedings, Windpower '98*, pp. 291-304.
27. Lobitz, D. and Veers, P., "Aeroelastic Behavior of Twist-coupled HAWT Blades," *Proceedings, ASME/AIAA Wind Energy Symposium*, Reno, NV, 1998, pp. 75-83.
28. Lobitz, D. and Laino, D., "Load Mitigation with Twist-coupled HAWT Blades," *Proceeding ASME/AIAA Wind Energy Symposium*, Reno, NV, 1999, pp. 124-134.
29. D. Lobitz, P. S. Veers and D. J. Laino, "Performance of Twist-Coupled Blades on Variable Speed Rotors," *Proceedings, ASME/AIAA Wind Energy Symposium*, Reno, NV, 2000, pp. 404-412.
30. D. W. Lobitz et al., *The Use of Twist-Coupled Blades to Enhance the Performance of Horizontal Axis Wind Turbines*, SAND2001-1303, May 2001.
31. D. Griffin, *Evaluation of Design Concepts for Adaptive Wind Turbine Blades*," SAND2002-2424, Sandia National Laboratories Contractor Report, Albuquerque, NM, August 2002.
32. D. Berry, *Design of 9-Meter Carbon-Fiberglass Prototype Blades: CX-100 and TX-100*, SAND2007-0201, Sandia National Laboratories, Albuquerque, NM, September 2007.

33. White D., Musial, W., Engberg, S. "Evaluation of the New B-REX Fatigue Testing System for Multi-Megawatt Wind Turbine Blades" *Proceeding, ASME/AIAA Wind Energy Symposium*, Reno, NV, 2005
34. Rumsey, M. and Paquette J., "Experimental Results of Structural Health Monitoring of Wind Turbine Blades," 46th AIAA Aerospace Sciences Meeting and Exhibit, Reno, NV, 2008.
35. J. Paquette, J. van Dam and S. Hughes "Structural Testing of 9 m Carbon Fiber Wind Turbine Research Blades," [45th AIAA Aerospace Sciences Meeting and Exhibit, Reno, NV, 2007.](#)
36. J. Paquette, J. van Dam, S. Hughes and J. Johnson, "Fatigue Testing of 9 m Carbon Fiber Wind Turbine Research Blade," [46th AIAA Aerospace Sciences Meeting and Exhibit, Reno, NV, 2008.](#)

APPENDIX A: Selected Material Definitions

1. QQ1. E-glass/epoxy laminate based on 0° Fabric B and ±45° Fabric F
 Lay-up and % 0°-material: [$\pm 45/0_2$]_s, 64%-0°
 Fiber volume fraction and thickness: 0.53 and 4.09 mm
 Matrix: epoxy (Vantico TDT 177-155)
 Process, cure, and post-cure temperatures: VARTM, RT, 6 hours at 70°C
 Laminate fabricated by: MSU

2. E-LT-5500-EP. E-glass/epoxy laminate based on 0° fabric D and ±45° Fabric G
 Lay-up and % 0° material: [$\pm 45/0/\pm 45/0/\pm 45$], 66%-0°
 Fiber volume fraction and thickness: 0.55 and 4.59 mm
 Matrix: epoxy (Huntsman Araldite LY1564/hardener XB3485)
 Process, cure and post-cure temperature: Infusion (TPI SCRIMP™), 60°C and 82°C
 Fabricated by: TPI (Supplied by Global Energy Concepts (GEC)/BSDS Program (11))

3. WS1. WindStrand™ fiber/epoxy
 Lay-up and %-0° material: [$\pm 45/0/\pm 45$], 50%-0°
 Fiber volume fraction and thickness: 0.61 and 2.56 mm
 Matrix: epoxy (MGS L135i/137i)
 Reinforcement (0 and ±45): WindStrand™ 17-1200 SE2350M2 strands (2000 g/m²) and DB1000 (same strands)
 Process, cure and post-cure temperature: vacuum infusion, 35°C, 90°C
 Laminate fabricated by: Owens Corning

4. P2B. Prepreg hybrid carbon-glass (dispersed fibers in 0° plies, fabric in ±45°s)
 Lay-up and %-0° material: [$\pm 45/0_4$]_s, 85%-0°
 Fiber volume fraction and thickness: 0.55 and 2.75 mm
 Prepreg: 0°-Newport NCT-307-D1-34-600 carbon; ±45°-NB307-D1-7781-497A Glass
 Process and cure conditions: vacuum bag, 3 hrs. at 121°C
 Laminate fabricated by: MSU

5. MMWK-C/G-EP. Infused carbon/glass triax hybrid, Fabric H

Lay-up and %-0° material: [(45/0/-45)₄], 75%-0° (by volume)
Fiber volume fraction and thickness: 0.56 and 4.3 mm
Matrix: epoxy (Jeffco 1401)
Process, cure and post-cure temperature: TPI SCRIMP™ infusion, 60°C and 82°C
Laminate fabricated by: TPI (supplied by GEC/BSDS program (11))

6. CGD4E. VARTM carbon/glass hybrid, Fabrics A and I

Lay-up and %-0° material: [$\pm 45/0_3/\pm 45$], 76%-0°
Fiber volume fraction and thickness: 0.50 and 2.61 mm
Matrix: epoxy (SP Systems Prime 20)
Process, cure and post-cure temperature: VARTM, 20°C and 70°C
Laminate fabricated by: MSU